Experimental Measurements of the Current, Temperature, and Density Profile Changes during a Disruption in the DIII-D Tokamak

P. L. Taylor, A. G. Kellman, B. W. Rice, and D. A. Humphreys
General Atomics, P.O. Box 85608, San Diego, California 92186-9784
(Received 10 October 1995)

The first simultaneous measurements of the current, temperature, and density profile changes during a disruption have now been made on the DIII-D tokamak. In radiative collapse disruptions the current profile measured using the motional Stark effect diagnostic is observed to flatten rapidly (~1.2 ms) at the final stage of a 10 ms thermal quench and just prior to the start of the current quench. The current flattening is faster than can be explained by relaxation due to classical or neoclassical resistive processes.

PACS numbers: 52.55.Fa

Tokamak discharges are frequently ended by disruptions [1–5], an instability leading to a very sudden termination of the plasma. Disruptions can result in large currents and forces in the containment vessel, concentrated energy deposition on the plasma facing wall from runaway electrons, and high heat fluxes due to the rapid loss of stored energy. These issues are a considerable concern for future fusion devices such as ITER, where the forces and energy deposition can be both the major design consideration and a limitation on the physics capability of the device. Although numerous studies of disruptions have been made [1–5], critical data are still needed to develop theoretical models for fundamental aspects of the disruption. Previous experiments [6–9] which reported profile measurements of the temperature, density, or current at the disruption were either limited to only a partial set of the profiles or the measurements did not cover all of the disruptive phases. This Letter describes simultaneous profile measurements of the current, temperature, and density during the disruptive phase of a beam heated single-null divertor discharge in the DIII-D tokamak.

In DIII-D, radiative collapse disruption experiments were carried out by forcing a disruption with the injection of an impurity gas (argon). The disruptions were timed to occur with diagnostics optimized at the time of the disruption. The deuterium discharges were lower single-null divertors with plasma current $I_p = 1.5$ MA, toroidal field $B = 2.1$ T, major radius $R = 1.7$ m, minor radius $a = 0.61$ m, and an elongation of 1.8. Neutral deuterium beam heating was used with a power of 12 MW, and the plasma was in H mode at the time of the gas injection.

An argon gas puff of 40 ms duration, with a total of ~2 Torr l of gas, caused a disruption approximately 60 ms after the start of the gas injection (Fig. 1). If all the argon entered the plasma and was fully stripped, the argon density would represent ~5% of the plasma density and the calculated effective charge Z_{eff} would be ~18. The radiated power, due to this large amount of argon, exceeds the 12 MW input power approximately 16 ms after the start of the gas injection, rises rapidly after the start of the thermal quench, and eventually exceeds 100 MW. The radiated power profile shows the radiation is in the outer 20% to 30% of the plasma before the disruption and outside the separatrix around the time the current quench starts; the 8 ms average of the bolometer data precludes an exact correlation of the radiation with disruption events. As the gas is injected and the radiated power increases, a rotating $n = 1$ mode becomes stationary (locked) and starts to grow ~2 ms before the thermal quench starts (note poloidal magnetic field perturbations in Fig. 2). The thermal quench begins (Fig. 2, 2.035 s) with the crash of the central soft x ray and the decrease in the calculated stored energy. Most of the stored energy is lost in the first 5 ms of the thermal quench. In these discharges, some reheating of the central plasma occurs which peaks the current profile (note the increase of the internal inductance l_i at 2.039–2.044 s). This is followed by the final and more rapid thermal quench at 2.044 s and the start of the current quench at 2.045 s. The locked

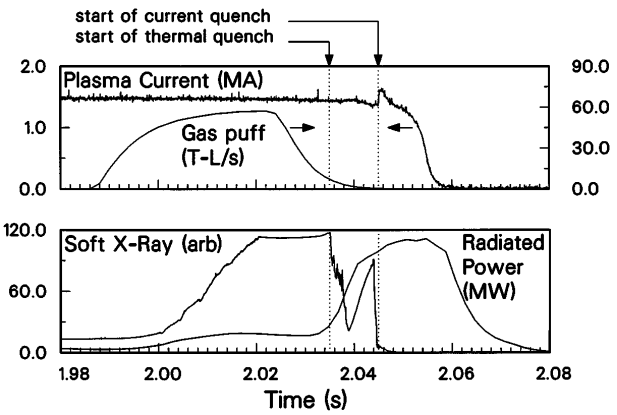

FIG. 1. Time evolution of discharge 81167 showing plasma current, argon gas puff, central soft x ray, and the total radiated power (averaged over 8 ms). The start of the thermal quench and the start of the current quench are marked. Note the soft x-ray signal is saturated before the start of the thermal quench but recovery from saturation is not delayed.

 0031-9007/96/76(6)/916(4)$06.00

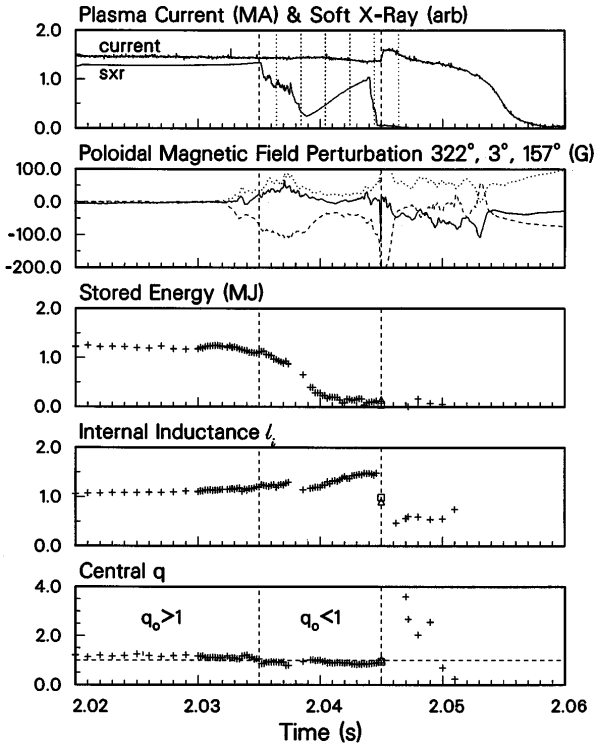

FIG. 2. Time evolution of discharge 81167 showing plasma current and central soft x ray, the nonaxisymmetric part of the poloidal magnetic field perturbation at three toroidal angles (322° = solid, 3° = dotted, 157° = dashed), plasma stored thermal energy, internal inductance l_i, and the q on the magnetic axis. The cross symbols are the results of the equilibrium fit averaged over 0.2 ms and use magnetic probe arrays at two toroidal locations, except for the triangle and square results which each use only one of the magnetic probe arrays. The start of the thermal and current quenches is marked with the dashed lines, and the Thomson scattering profile times of Fig. 3 are marked by the dotted lines.

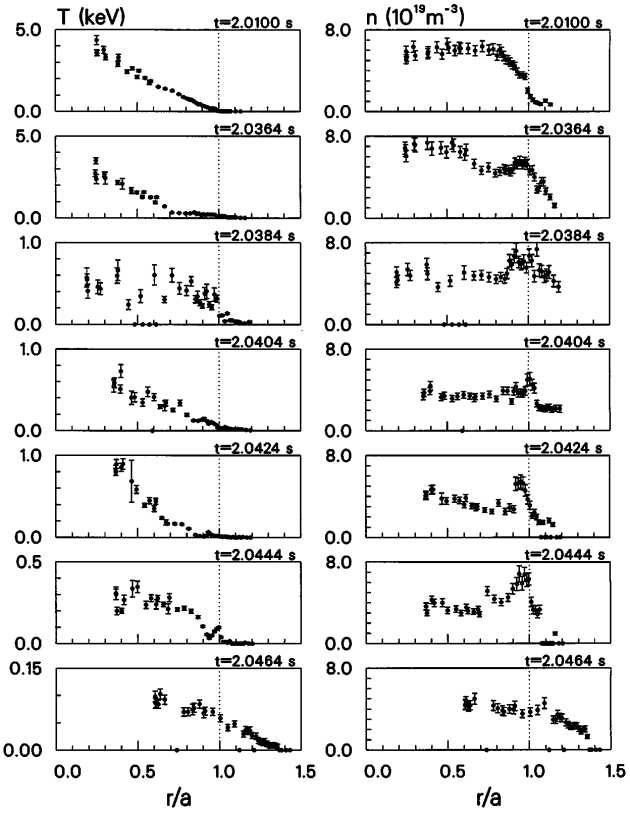

FIG. 3. Thomson scattering electron temperature and density profiles at the times marked in Fig. 2 for discharge 81167 vs the normalized radius. Note the change of vertical scale with time for the temperature plots. The plasma edge (separatrix boundary) is shown by the vertical dotted line.

mode is large during the energy loss from 2.035–2.039 s, then decreases, allowing the reheating to occur, and has a rapid growth during the final thermal quench leading into the start of the current quench. These discharges are not sawtoothing, and the central safety factor q_0 is slightly above 1 until the thermal quench begins when q_0 drops below 1. (Note the q error bars are less than the symbol size in Fig. 2.)

The electron temperature and density profile measurements were made using the Thomson scattering system by triggering each of six lasers at preset times through the disruption. This system measures the temperature and density profiles at 40 spatial points on a vertical chord passing through the plasma at $R = 1.94$ m (initial plasma center at $R = 1.76$ m).

At the thermal quench the temperature inside the last closed flux surface drops, and a cold edge region, which may have been developing due to the high radiation, is evident (Fig. 3, 2.036 s). The central temperature 2 ms later has dropped from the original 4 keV to 600 eV, and at 2.039 s the center starts to reheat with the central temperature reaching almost 1 keV at 2.0424 s. In the middle of the final thermal quench, 2.0444 s, the temperature has collapsed to approximately 300 eV, and at 2.0464 s, after the start of the current quench, the temperature is less than 100 eV. At 2.0384 s, near the minimum of the central stored energy during the thermal quench and before the central reheating starts, the large variations in the temperature with position may indicate that the plasma is stochastic. This behavior is also seen to a lesser degree at 2.0444 s during the final thermal quench, but is not seen in the other profiles.

During the thermal quench, the density profile develops a peak at the edge. The central density falls by almost 50% partially balancing the increase in edge density, which remains high until after the start of the current quench. The total number of particles increases ~15% during the energy loss (2.035–2.039 s), decreases during the reheating to ~70% of the initial number, and increases again from the final thermal quench through the start of the current quench to ~80% of the initial number. Note that the peak in density remains at the plasmas edge

even though the edge (separatrix boundary at $r/a = 1$) has moved from $z = 0.92$ m at 2.010 s to $z = 0.66$ m at 2.0464 s due to the plasma moving vertically downward and radially inward.

The data also show some interesting behavior of the plasma in the scrapeoff layer (SOL) ($r/a > 1$). During both energy loss periods (2.0364–2.0384 and 2.0444 s) the temperature and density in the SOL increase significantly; temperature ~100 eV at $r/a = 1$ with density ~2 times larger over much of the SOL. At 2.0464 s, after the start of the current quench, both the temperature and density profiles have broadened leaving a large region of plasma outside the separatrix.

The current density profile is determined from the measurements and equilibrium reconstruction using the code EFITD [10] which fits a solution of the Grad-Shafranov equation to several measured quantities including the poloidal field and flux on the vacuum vessel wall, external coil currents, and the pitch angle of the internal magnetic field measured at 16 radial points near the vertical midplane using the motional Stark effect (MSE) diagnostic [11,12]. The reconstruction also includes induced currents flowing in the vacuum vessel wall. The sampling rate used for the magnetics data was 5 kHz (typical bandwidths 50 kHz) and the MSE system which has a response time of ~1 ms was sampled at 2 kHz. Examples of the MSE measured vertical field in the plasma, the resulting fit from the magnetohydrodynamic (MHD) equilibrium calculation, and current profile are shown in Fig. 4. The current profile flattens suddenly after the final thermal quench as seen in the rapid decrease of the internal inductance prior to the current quench (Fig. 2). The increase in total plasma current after the current quench starts is driven by this rapid decrease in the internal inductance. Calculations indicate, as expected, that the less restrictive conservation of magnetic energy accounts for the measured current increase better than the more restrictive conservation of flux. The current increase is 0.24 MA, and a calculation of the current increase, assuming the magnetic energy ($E = \frac{1}{2}\int_{V_p} \vec{A}\cdot\vec{J}dV \equiv \frac{1}{2}L_p I_p^2$ with $\vec{A}$, $\vec{J}$ the vector potential and current density, respectively, and L_p, I_p, V_p the plasma inductance, current, and volume) is conserved, gives 0.21 MA, while a calculation of the current increase, assuming the current average poloidal magnetic flux ($\langle\Psi_p\rangle_{J_\phi} = I_p^{-1}\int J_\phi \Psi_p dA_{\text{poloidal}} \equiv L_p I_p$ with J_ϕ the toroidal current, Ψ_p the poloidal magnetic flux) is conserved, predicts a current increase of 0.43 MA. Note that the current profile flattening occurs only at the end of the final thermal quench despite most of the energy loss occurring after the start of the thermal quench. The current profile change from before the disruption ($t = 2.030$ s) to after the start of the current quench ($t = 2.048$ s) also shows the flattening (Fig. 4).

The EFITD reconstructions which give the inductance, stored energy, and q (Fig. 2) assume the plasma is axisymmetric, and the analysis uses data from magnetic probe arrays at two toroidal locations separated by 105° and MSE data from an intermediate toroidal location. The lack of data in Fig. 2 around 2.038 and 2.045 s is due to poor MHD equilibrium fits at these times and may be indicative that the plasma axisymmetry is poor or that the plasma is stochastic. The lack of axisymmetry is seen in both the $n = 1$ locked mode amplitude which is large at these times and in the differences in the poloidal magnetic field measurements from two arrays at different toroidal locations; differences that are normally less than 1% increase to 9% at 2.038 s (largest variation at the outboard midplane location) and to 14% at 2.045 s. The variations near 2.038 s in the temperature profile and in the MSE measured vertical field profile (Fig. 4) tends to indicate the plasma is stochastic. A unique feature of this discharge also occurs around 2.038 s; the position of the magnetic axis of the plasma (from MSE measurements) has moved outward by 10 cm at the same time that external coils show that the geometric centroid and the current centroid have moved inward by 2–5 cm. A smaller, but similar effect is seen at ~2.045 s. The EFITD equilibrium reconstructions at 2.045 s (Fig. 2) with reasonable accuracy for the fits could only be obtained by using just one of the magnetic probe arrays with the MSE data and were done to obtain an intermediate point on the l_i curve. Although from equilibrium considerations it would be expected that the plasma would shift inward following the energy loss, the large outward movement

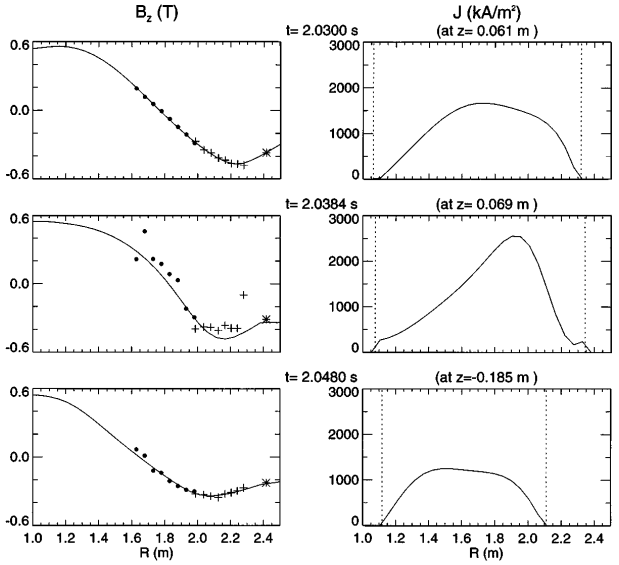

FIG. 4. Vertical field (B_z) measured by the MSE central array (dots), outer array (crosses), and a probe on the vessel wall (star) along with the equilibrium fit (curve) and the current profile (J) from the equilibrium fit. The vertical position of the magnetic axis where the current profile is calculated is noted. Examples from three times are shown including $t = 2.0384$ s, where the equilibrium fit to the MSE data is poor and the results are rejected.

of the magnetic axis indicates either a kink instability or outwardly shifted island structure at the plasma center.

These initial DIII-D experiments performed for radiative collapse disruptions provide measurements on the temperature, density, and current profile to better describe the disruption process. An $n = 1$ locked mode is a precursor to the disruption, then a two-phase thermal quench occurs, followed by the current quench. During the initial phase of the thermal quench, there is a slow ($\sim$5 ms) loss of most ($\sim$75%) of the energy with little change in the configuration; the central q decreases slightly as it drops below 1, and the current profile is relatively unchanged. In the second phase of the thermal quench there is a slow reheating of the center followed by a rapid loss of the remaining energy ($\leq$1 ms) with a rapid flattening of the current profile ($\sim$1.2 ms). After the stored energy is lost early in the thermal quench the central temperature is a few hundred eV, and after the start of the current quench the temperature has fallen to the 100 eV level.

The current flattening is faster than can be explained by relaxation due to classical or neoclassical resistive processes. In order for the current profile to flatten on the observed time scale of 1.2 ms through resistive diffusion, the effective resistivity would have to be $\sim$15 times the Spitzer value (assuming $T_e \sim 100$ eV, $Z_{\text{eff}} \sim 6$). The calculated enhancement in resistivity must, in fact, be even greater than this, since T_e is decreasing from 300 to 100 eV during the current redistribution interval. Even assuming the maximum upper bound of $Z_{\text{eff}} \sim 18$ requires an effective resistivity $\sim$5 times the Spitzer value to account for the observed relaxation time. A calculation of the neoclassical resistivity yields an increase of approximately 20% over the Spitzer value. The neoclassical effects of toroidicity and trapped electrons therefore cannot account for the large effective resistivity required. This implies that the magnetic transport during the rapid current flattening is anomalous, consistent with resistive MHD-driven field line reconnection and stochastization in the plasma core following the thermal quench.

This work was sponsored by the U.S. Department of Energy, under Contract No. DE-AC03-89ER51114. We gratefully acknowledge the assistance of L. L. Lao, A. W. Leonard, R. E. Stockdale, discussions with T. E. Evans, A. W. Hyatt, and E. J. Strait, and the contributions of the DIII-D Operations staff.

[1] J. A. Wesson *et al.,* Nucl. Fusion **29**, 641 (1992).
[2] D. J. Ward and J. A. Wesson, Nucl. Fusion **32**, 1117 (1992).
[3] TFR Group Collaboration, Nucl. Fusion **25**, 919 (1985).
[4] R. G. Kleva and J. F. Drake, Phys. Fluids B **2**, 372 (1991).
[5] R. Yoshino *et al.,* Nucl. Fusion **33**, 1599 (1993).
[6] E. D. Frederickson *et al.,* Nucl. Fusion **33**, 141 (1993).
[7] M. Abe *et al.,* J. Plasma Fusion Res. **69**, 352 (1993).
[8] A. Janos *et al., Plasma Physics and Controlled Nuclear Fusion Research 1992*, Proceedings of the 14th International Conference, Wurzburg (International Atomic Energy Agency, Vienna, 1993), Vol. 1, p. 527.
[9] Z. A. Pietrzyk *et al.,* Nucl. Fusion **32**, 1735 (1992).
[10] L. L. Lao *et al.,* Nucl. Fusion **30**, 1035 (1990).
[11] D. Wroblewski and L. L. Lao, Rev. Sci. Instrum. **63**, 5140 (1992).
[12] B. W. Rice *et al.,* Rev. Sci. Instrum. **66**, 373 (1995).